The fluid sloshing in a vertical circular cylindrical tank with a rigid-ring baffle II: Nonlinear resonant waves*

I. Gavrilyuk[1], I. Lukovsky[2], Yu. Trotsenko[2] and A. Timokha[2†]

[1] *Berufakademie Thüringen-Staatliche Studienakademie, Am Wartenberg 2, 99817, Eisenach, Germany;*
[2] *Institute of Mathematics, National Academy of Sciences of Ukraine, Tereschenkivska 3, 01601 Kiev, Ukraine*

Abstract

Nonlinear resonant fluid sloshing in a circular cylindrical tank, which contains a rigid-ring baffle, is examined by using a nonlinear asymptotic modal method. The overall fluid depth is fairly deep (depth/radius ratio ≥ 1) and relevant restrictions to the distance between baffle and hydrostatic fluid plane are introduced to avoid baffle's slopes. A nonlinear modal system is derived. It couples five natural modes and extends earlier results for circular cylindrical tanks without baffles. Derivation of the modal system utilises numerical-analytical solutions of the linear sloshing problem obtained in earlier authors' paper. The main emphasis is placed on quantifying steady-state wave motions versus the size and the location of the baffle. A forthcoming paper will study nonlinear damping due to vorticity stress at the sharp baffle edges and generalise the present modal technique.

Keywords: *Fluid sloshing, Rigid baffle, Nonlinear modal system, Steady-state solutions*

MSC (1991): 35R35, 76B07

Introduction

Tanks with baffles, which suppress mobility of a fluid cargo, are typical attributes of various industrial applications. Being intended for mitigating hydrodynamic loads, installation of baffles increases the overall structural damping, prevents wave impacts and slamming. Since the sloshing behaviour depends on the shape, the location and the number of baffles, testing

*The work is partially supported by DFG.

†The author acknowledges sponsorship by the Alexander von Humboldt Foundation and the Centre for Ship and Ocean Structures, NTNU, Norway

is a very tedious and expensive task when studying the numerous design scenarios. The task becomes simpler for non-resonant sloshing when fluid motions can be evaluated in the framework of linear theories. However, relevance of resonant sloshing associated with the closeness of the lowest sloshing frequency to a control structural frequency is a great motivation to develop numerical tools for fully nonlinear free boundary problems.

Resonant sloshing behaviour may be strictly dissipative, accompanied by flow separation at the baffle edge and even discontinuity of the fluid volume. This happens for instance in ship tanks on realistic seaway. Study of such a behaviour disallows analytical approaches and there is only a limited set of numerical tools providing robust simulations (Cariou & Casella [4], Colagrossi & Landrini [9]). Sloshing demonstrates another behaviour for fairly deep fluid fill levels and small-amplitude (structural) vibrations of the carrier. It is not so strongly dissipative and the vorticity is perceptible only in small vicinity of the baffle edge to influence the ambient flows. Such sloshing behaviour appears, for instance, in some spacecraft applications and building industry (connected with the Tuned Sloshing Dampers). As matter of fact, major of the Computational Fluid Dynamics (CFD) methods focuses on simulating this type of sloshing. By computing an appropriate Cauchy problems (see recent examples by Celebi & Akyildiz [5], Cho & Lee [6, 7, 8] and surveys by Ibrahim *et al.* [21], introductory section by Gavrilyuk *et al.* [19][‡]), the CFD methods showed quite efficient simulations of transient waves on short-time scale. However, they are quite limited in quantifying steady-state (periodic) solutions which appear after 200-300 forcing periods. Prediction of stable steady-state motions by the CFD methods is especially difficult and tedious task for three-dimensional waves when different steady-state wave regimes co-exist for the same physical parameters and there is a frequency domain where all the regimes are not stable: these methods cannot distinguish "chaotic" motions (occurring in the latter frequency domain) and the numerical instability.

Selection of stability zones for resonant steady-state solutions (this procedure is called the classification, Faltinsen *et al.* [12]) belongs to the most important engineering task. The classification makes it possible to predict the types of hydrodynamic loads and, after testing different tank shape, to find an optimal structural design. Since traditional CFD methods run into serious difficulties to perform the classification, it has been doing by analytical methods finalised by experimental tests. Typically, analytical predictions are based on linear sloshing theories, but the current scientific literature contains some nonlinear analytically-oriented approaches which combine asymptotic and modal methods. The background of these approaches for smooth (without baffles) tanks is in some detail described by Miles [28, 29], Lukovsky [24], Gavrilyuk *et al.* [18], Faltinsen *et al.* [13, 10] and Faltinsen & Timokha [16]. To the authors best knowledge, the present pioneering study represents the first attempt expanding the nonlinear approaches to tanks with baffles.

We consider an inviscid fluid partially filling a circular cylindrical tank with an annular horizontal rigid baffle. Applicability of the ideal fluid model for weakly-nonlinear sloshing is confirmed by experiments and numerical simulations by Bogoryad & Druzhinina [1], Mikishev [26], Mikishev & Churilov [27] and Cho & Lee [7]. The fluid damping (due to viscosity and vorticity stress at the sharp edge) plays the secondary role for relatively small wave amplitudes. Of course, its importance growths with increasing the amplitudes, but, even in that case, the classification of forced steady-state waves remains qualitatively the

[‡]Furthermore, Part 1

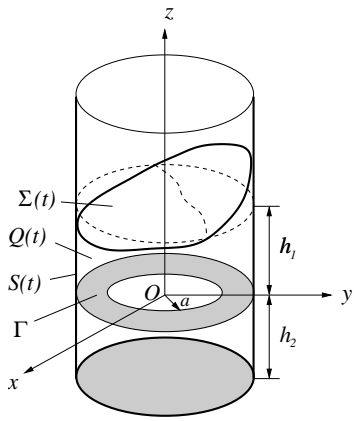

Fig. 1. The sketch of a circular cylindrical tank with partially filled by a fluid.

same. This has been defended by Miles [28, 29], Faltinsen *et al.* [15, 12, 11] and Hill [20] by operating with damping terms in modal systems for sloshing in smooth tanks. Appropriate generalisations for tanks with baffles will be presented in the forthcoming paper. Buzhinkii's [3] formula on damping rates due to vorticity stress is useful in this context.

We start with short introductory description of an asymptotic modal scheme by Narimanov [31]. Using this scheme derives a five-dimensional system of ordinary differential equations (modal system) governing nonlinear resonant waves due to horizontal tank's vibration with frequencies close to the lower natural modes. The modal system is based on the third-order Moiseyev ordering. This ordering has widely been explored in nonlinear modal analysis. Its justification was done by Lukovsky [24] and Miles [28, 29]. One should note, that derivation of the modal system is facilitated by results of the authors earlier paper (Part 1), where accurate analytically-oriented methods for approximating the natural linear modes (complex amplitudes) is proposed. The physical and numerical limitations of the nonlinear modal system are extensively discussed.

1. Nonlinear modal theory

1.1. Free boundary problem

Let a rigid circular base cylindrical tank of the radius R be partially filled by a fluid with the mean depth h. The inner periphery of the tank is equipped by a thin rigid-ring baffle which divides the overall height h into h_1 and h_2, where h_1 is the height of fluid layer over the baffle in its hydrostatic state and h_2 is the length between the baffle and the flat bottom. Thickness of the baffle is neglected. Fluid motions occurring due to either initial perturbations of the planar hydrostatic equilibrium or tank's oscillations are furthermore described in the framework of an inviscid model with irrotational flows. Waves magnitude is assumed to be small relative to h_1 to keep the baffle inside of the fluid bulk (sloshing does not slope baffle).

The problem is studied in size-dimensionless statement suggesting that all the lengths

and physical constants are normalised by the base radius R. This implies in particular that $h_1 := h_1/R, h_2 := h_2/R, g := g/L_1$ (gravity acceleration g has the dimension $[s^{-2}]$) etc. Corresponding free boundary problem is formulated in the tank-fixed coordinate system $Oxyz$ (see, Moiseyev & Rumyantsev [34], Narimanov *et al.* [32] and Lukovsky & Timokha [25]). Without loss of generality, the Oz-axis is directed along the symmetry axis and the origin O is posed in the baffle plane as shown in Figure 1. Further, the analysis will be restricted to the prescribed horizontal tank oscillations along the Ox-axis that are governed by a given time-dependent vector $\boldsymbol{v}_O(t) = (v_{1O}(t), 0, 0)^T$ implying translatory velocity of the mobile coordinate system relative to an absolute coordinate system $O'x'y'z'$.

Under these assumptions the governing free boundary problem takes the following form

$$\begin{aligned}
&\Delta\Phi = 0 \quad \text{in } Q(t); \quad \frac{\partial\Phi}{\partial\nu} = \boldsymbol{v}_O \cdot \boldsymbol{\nu} \quad \text{on } S(t) \cup \Gamma, \\
&\frac{\partial\Phi}{\partial\nu} = \boldsymbol{v}_O \cdot \boldsymbol{\nu} + \frac{f_t}{\sqrt{1+(\nabla f)^2}} \quad \text{on } \Sigma(t); \quad \int_{Q(t)} dQ = \text{const}, \\
&\frac{\partial\Phi}{\partial t} + \frac{1}{2}(\nabla\Phi)^2 - \nabla\Phi \cdot \boldsymbol{v}_O + gf = 0 \quad \text{on } \Sigma(t),
\end{aligned} \tag{1.1}$$

where the unknowns are the function $f(x, y, t)$ defining the free surface evolution $\Sigma(t)$: $z = f(x, y, t)$ and the absolute velocity potential $\Phi(x, y, z, t)$ which should be calculated in time-varying fluid volume $Q(t)$ confined to the wetted body surface $S(t)$, the baffle Γ and $\Sigma(t)$; $\boldsymbol{\nu}$ is outward normal to $Q(t)$.

This papers examines the case of resonant harmonic forcing, i.e.

$$v_{O1}(t) = -\sigma\epsilon \sin\sigma t, \tag{1.2}$$

where $\epsilon \ll 1$ is the non-dimensional excitation amplitude and $\sigma \to \omega_1^{(1)} = \sqrt{g\kappa_1^{(1)}}$ ($\omega_1^{(1)}$ is the lowest sloshing frequency).

The evolutional free boundary problem (1.1) should be completed by either initial or periodicity conditions. The initial (Cauchy) conditions assume

$$f(x, y, t_0) = f_0(x, y); \quad \left.\frac{\partial\Phi}{\partial\nu}\right|_{z=f_0(x,y)} = \Phi_0(x, y, z) \tag{1.3}$$

to be known at $t = t_0$. The periodicity conditions are in many applied problems associated with periodicity of wave pattern and velocity field, i.e.

$$f(x, y, t+T) = f(x, y, t); \quad \nabla\Phi(x, y, z, t+T) = \nabla\Phi(x, y, z, t), \tag{1.4}$$

where $T = 2\pi/\sigma$.

1.2. Third-order asymptotic scheme by Narimanov

The nonlinear asymptotic modal modelling and its modifications were reported by Lukovsky [24], Lukovsky & Timokha [25], Faltinsen *et al.* [13] and La Rocca *et al.* [22, 23]. Furthermore, we follow the original scheme by Narimanov [31, 32]. It introduces the following

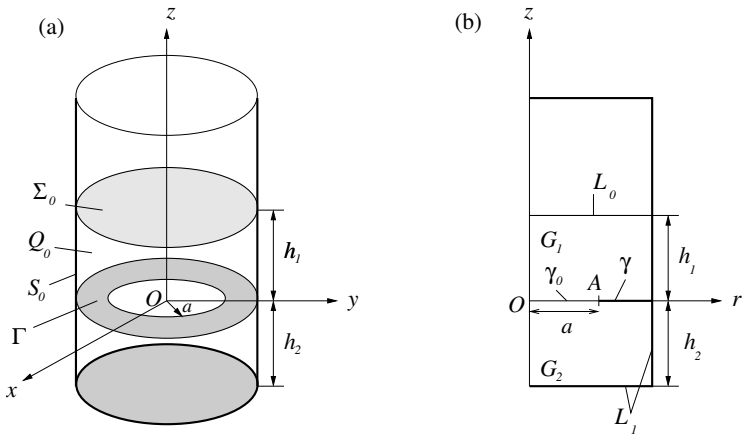

Fig. 2. Hydrostatic fluid shape in a rigid cylindrical tank; three-dimensional and meridional sketches. A thin rigid-ring baffle Γ is permanently submerged into the fluid volume.

solution of (1.1) (in cylindrical coordinate system $Or\eta z$)

$$
\begin{aligned}
f(r,\eta,t) &= \sum_{m=0}^{\infty}\sum_{i=1}^{\infty}\left(\beta^s_{m,i}(t)\sin\eta+\beta^c_{m,i}(t)\cos\eta\right)\tilde{F}^{(m)}_i(r,\eta),\\
\Phi(r,\eta,z,t) &= -\,r\sigma\epsilon\,\cos(\theta)\sin(\sigma t)+\\
&\quad+\sum_{m=0}^{\infty}\sum_{i=1}^{\infty}\left(\frac{d\beta^s_{m,i}(t)}{dt}\phi^{(m,s)}_i(r,\eta,z,t)+\frac{d\beta^c_{m,i}(t)}{dt}\phi^{(m,c)}_i(r,\eta,z,t)\right).
\end{aligned}
\tag{1.5}
$$

Here, $\beta^s_{m,i}(t)$ and $\beta^c_{m,i}(t)$ are the unknown modal functions and $\tilde{F}^{(m)}_i(r,\eta)=F^{(m)}_i(r)\begin{matrix}\sin\\ \cos\end{matrix}\eta$, $m=0,\ldots;\ i=1,\ldots$ are the normalised linear surface modes defined in Part 1 as

$$
F^{(m)}_i(r)=\frac{\kappa^{(m)}_i\psi^{(m)}_i(r,0)}{\psi^{(m)}_i(1,0)},\quad m=0,\ldots;\ i=1,\ldots,
$$

where $\psi^{(m)}_i(r,z)\begin{matrix}\sin\\ \cos\end{matrix}\eta$ are the fundamental solutions (complex amplitudes) in Q_0 (see, Figure 2).

Representation (1.5) needs solutions of the Neumann boundary value problem

$$
\Delta\phi_F=0\ \text{ in } Q(t);\quad \frac{\partial\phi_F}{\partial\nu}=0\ \text{ on } S(t) \text{ and } \Gamma;\quad \frac{\partial\phi_F}{\partial\nu}=\frac{F(r,\eta)}{\sqrt{1+(\nabla f)^2}}\ \text{ on } \Sigma(t) \tag{1.6}
$$

where $F(r,\eta)$ coincides with either $F^{(m)}_i(r)\sin\eta$ or $=F^{(m)}_i(r)\cos\eta$. In the first case, $\phi_F=\phi^{(m,s)}_i$ and the second case implies $\phi_F=\phi^{(m,c)}_i$.

Since solutions of (1.6) depend parametrically on $\Sigma(t):\ z=f(r,\eta,t)$, by assuming small deviations of the free surface, Narimanov solves (1.6) asymptotically and defines the

following series by $\{\tilde{\beta}_{m,i}(t)\} = \{\beta^s_{m,i}(t)\} \cup \{\beta^c_{m,i}(t)\}$

$$\phi_F(r,\eta,z,t) = \phi^{(0)}_F(r,\eta,z) + \sum_{m=0}^{\infty}\sum_{i=1}^{\infty} \tilde{\beta}_{m,i}\phi^{(1)}_{F,mi}(r,\eta,z) + \\ + \sum_{m,n=0}^{\infty}\sum_{i,j=1}^{\infty} \tilde{\beta}_{m,i}\tilde{\beta}_{n,j}\phi^{(2)}_{F,mi,nj}(r,\eta,z) + \ldots. \quad (1.7)$$

Here, $\phi^{(0)}_F(r,\eta,z)$, $\phi^{(1)}_{F,mi}(r,\eta,z)$, $\phi^{(2)}_{F,mi,nj}(r,\eta,z)$ etc. can be found from a recursive Neumann boundary value problems in the static domain Q_0 (Narimanov [31, 32] and Lukovsky [24]) with zero-boundary condition on S_0 and non-zero conditions on Σ_0 (see, Figure 2). Each a Neumann problem has analytical solutions in terms of a Fourier series with natural modal basis $\psi^{(m)}_i(r,z)\begin{matrix}\cos\\ \sin\end{matrix}\eta$ (see, the spectral theorems by Feschenko *et al.* [17]). An accurate numerical-analytical approximation of $\psi^{(m)}_i(r,z)\begin{matrix}\cos\\ \sin\end{matrix}\eta$ has been obtained in Part 1.

1.3. Finite-dimensional nonlinear modal system, its applicability

As shown by Narimanov [31] (circular cylindrical tank), Moiseyev [30] (rectangular tank) and Faltinsen & Timokha [10] (square-base tank) resonant excitations of the lowest natural modes lead to the following ordering of the modal functions:

$$\beta^c_{1,1} \sim \beta^s_{1,1} = O(\epsilon^{1/3}), \quad \beta^c_{2,i} \sim \beta^s_{2,i} \sim \beta^c_{0,i} \sim \beta^s_{0,i} = O(\epsilon^{2/3}), \\ \beta^c_{j,i} \sim \beta^s_{j,i} \le O(\epsilon), \quad j \ge 3,\ i = 1,2,\ldots. \quad (1.8)$$

Adopting (1.8) in the Narimanov scheme implies the dominating pair of modal functions $\beta^c_{1,1}$, $\beta^s_{1,1}$ and the second-order modal functions $\beta^c_{2,i}$, $\beta^s_{2,i}$, $\beta^c_{0,i}$, $\beta^s_{0,i}$, $i = 1,2,\ldots$. Pursuing approximations of the free surface within to $O(\epsilon)$ makes it possible to neglect an infinite-dimensional set of higher-order modes. Lukovsky [24] (generic axial-symmetric tanks) and Miles [28, 29] (circular cylindrical tank) proposed and, by using numerous examples, defended the five-dimensional modal approximation

$$f(r,\eta,t) = \beta^c_{0,1}(t)F^{(0)}_1(r) + \left[\beta^s_{1,1}(t)\sin\eta + \beta^c_{1,1}(t)\cos\eta\right]F^{(1)}_1(r) + \\ + \left[\beta^s_{2,1}(t)\sin 2\eta + \beta^c_{2,1}(t)\cos 2\eta\right]F^{(2)}_1(r). \quad (1.9)$$

Miles [28, 29] showed that $\beta^c_{2,i}$, $\beta^s_{2,i}$, $\beta^c_{0,i}$, $\beta^s_{0,i}$, $i \ge 2$ contribute 10^{-4} into the overall kinetic energy of forced motions and their contribution may increase only in small vicinity of some isolated critical depths. Secondary (internal) resonances leading to amplification of higher modal functions will be discussed in the last section of the present paper.

Formal usage of (1.9) in Narimanov's scheme and neglecting $o(\epsilon)$ lead to the following system of nonlinear ordinary differential equations

$$\ddot{\beta}^s_{1,1} + \omega^{(1)}_1\beta^s_{1,1} + D_1((\beta^s_{1,1})^2\ddot{\beta}^s_{1,1} + \beta^s_{1,1}(\dot{\beta}^s_{1,1})^2 + \beta^s_{1,1}\beta^c_{1,1}\ddot{\beta}^c_{1,1} + \beta^s_{1,1}(\dot{\beta}^c_{1,1})^2) + \\ + D_2((\beta^c_{1,1})^2\ddot{\beta}^s_{1,1} + 2\beta^c_{1,1}\dot{\beta}^s_{1,1}\dot{\beta}^c_{1,1} - \beta^s_{1,1}\beta^c_{1,1}\ddot{\beta}^c_{1,1} - 2\beta^s_{1,1}(\dot{\beta}^c_{1,1})^2) - \\ - D_3(\beta^c_{2,1}\ddot{\beta}^s_{1,1} - \beta^s_{2,1}\ddot{\beta}^c_{1,1} + \dot{\beta}^s_{1,1}\dot{\beta}^c_{2,1} - \dot{\beta}^c_{1,1}\dot{\beta}^s_{2,1}) + D_4(\beta^s_{1,1}\ddot{\beta}^c_{2,1} - \beta^c_{1,1}\ddot{\beta}^s_{2,1}) + \\ + D_5(\beta^c_{0,1}\ddot{\beta}^s_{1,1} + \dot{\beta}^s_{1,1}\dot{\beta}^c_{0,1}) + D_6(\beta^s_{1,1}\ddot{\beta}^c_{0,1}) = 0, \quad (1.10a)$$

$$\ddot{\beta}^c_{1,1}+\omega^{(1)}_1\beta^c_{1,1}+D_1((\beta^c_{1,1})^2\ddot{\beta}^c_{1,1}+\beta^s_{1,1}\beta^c_{1,1}\ddot{\beta}^s_{1,1}+\beta^c_{1,1}(\dot{\beta}^s_{1,1})^2+\beta^c_{1,1}(\dot{\beta}^c_{1,1})^2)+$$
$$+D_2((\beta^s_{1,1})^2\ddot{\beta}^c_{1,1}-\beta^s_{1,1}\beta^c_{1,1}\ddot{\beta}^s_{1,1}+2\beta^s_{1,1}\dot{\beta}^s_{1,1}\dot{\beta}^c_{1,1}-2\beta^c_{1,1}(\dot{\beta}^s_{1,1})^2)+$$
$$+D_3(\beta^c_{2,1}\ddot{\beta}^c_{1,1}+\beta^s_{2,1}\ddot{\beta}^s_{1,1}+\dot{\beta}^s_{1,1}\dot{\beta}^s_{2,1}+\dot{\beta}^c_{1,1}\dot{\beta}^c_{2,1})-D_4(\beta^c_{1,1}\ddot{\beta}^c_{2,1}+\beta^s_{1,1}\ddot{\beta}^s_{2,1})+$$
$$+D_5(\beta^c_{0,1}\ddot{\beta}^c_{1,1}+\dot{\beta}^c_{1,1}\dot{\beta}^c_{0,1})+D_6(\beta^c_{1,1}\ddot{\beta}^c_{0,1})-\Lambda\ddot{v}_{O1}=0, \quad (1.10b)$$

$$\ddot{\beta}^c_{0,1}+\omega^{(0)}_1\beta^c_{0,1}+D_{10}(\beta^s_{1,1}\ddot{\beta}^s_{1,1}+\beta^c_{1,1}\ddot{\beta}^c_{1,1})+D_8((\dot{\beta}^s_{1,1})^2+(\dot{\beta}^c_{1,1})^2)=0, \quad (1.10c)$$

$$\ddot{\beta}^s_{2,1}+\omega^{(2)}_1\beta^s_{2,1}-D_9(\ddot{\beta}^s_{1,1}\beta^c_{1,1}+\ddot{\beta}^c_{1,1}\beta^s_{1,1})-2D_7(\dot{\beta}^s_{1,1}\dot{\beta}^c_{1,1})=0, \quad (1.10d)$$

$$\ddot{\beta}^c_{2,1}+\omega^{(2)}_1\beta^c_{2,1}+D_9(\ddot{\beta}^s_{1,1}\beta^s_{1,1}-\ddot{\beta}^c_{1,1}\beta^c_{1,1})+D_7((\dot{\beta}^s_{1,1})^2-(\dot{\beta}^c_{1,1})^2)=0, \quad (1.10e)$$

where $\omega^{(m)}_i=g\kappa^{(m)}_i$ and $D_i,\ i=1,\dots,10;\Lambda$ are functions of h_1,h_2 and a (see, Figure 2).

The coefficients $D_i,\ i=1,\dots,10$ and Λ are computed by

$$D_1=\frac{d_1}{\mu_{11}};\quad D_2=\frac{d_2}{\mu_{11}};\quad D_3=\frac{d_3}{\mu_{11}};\quad D_4=\frac{d_4}{\mu_{11}};\quad D_5=\frac{d_5}{\mu_{11}};\quad D_6=\frac{d_6}{\mu_{11}},$$
$$D_7=\frac{d_7}{\mu_{21}};\quad D_8=\frac{d_8}{\mu_{01}};\quad D_9=\frac{d_4}{\mu_{21}};\quad D_{10}=\frac{d_6}{\mu_{01}};\quad \Lambda=\frac{\lambda}{\mu_{11}}, \quad (1.11)$$

where $d_i,\ i=1,\dots,8$ and λ are determined by the integrals

$$d_1=\frac{\pi}{4}\int_{L_0}\left[(3\mathcal{G}_1+2\mathcal{G}_2)(F^{(1)}_1)^2+(3\mathcal{G}_2+4\mathcal{G}_5+2\mathcal{G}_6+2\mathcal{G}_7)\psi^{(1)}_1+\frac{3}{2}\frac{\partial^2\psi^{(1)}_1}{\partial z^2}\right]rdr,$$

$$d_2=\frac{\pi}{4}\int_{L_0}\left[(\mathcal{G}_1+4\mathcal{G}_2)(F^{(1)}_1)^2+(\mathcal{G}_3+2\mathcal{G}_5)\psi^{(1)}_1+\frac{1}{2}\frac{\partial^2\psi^{(1)}_1}{\partial z^2}(F^{(1)}_1)^3\right]rdr,$$

$$d_3=\frac{\pi}{2}\int_{L_0}\left(\mathcal{G}_{21}\psi^{(1)}_1+(F^{(1)}_1)F^{(2)}_1\right)rdr,$$

$$d_4=-\frac{\pi}{4}\int_{L_0}\left[\mathcal{G}_{12}\psi^{(1)}_1+(\mathcal{G}_1-\mathcal{G}_2)\psi^{(2)}_1+2(F^{(1)}_1)^2F^{(2)}_1\right]rdr,$$

$$d_5=\pi\int_{L_0}\left(\psi^{(1)}_1\mathcal{G}_{01}+(F^{(1)}_1)^2F^{(0)}_1\right)rdr,$$

$$d_6=\frac{\pi}{2}\int_{L_0}\left[\mathcal{G}_{01}\psi^{(1)}_1+(\mathcal{G}_1+\mathcal{G}_2)\psi^{(0)}_1+2(F^{(1)}_1)^2F^{(0)}_1\right]rdr,$$

$$d_7=d_4+\frac{1}{2}d_3;\quad d_8=d_6-\frac{1}{2}d_5;\quad \lambda=\pi\kappa^{(1)}_1\int_{L_0}r^2\psi^{(1)}_1dr,$$

$$\mu_{11}=\pi\int_{L_0}F^{(1)}_1\psi^{(1)}_1rdr;\quad \mu_{01}=2\pi\int_{L_0}F^{(0)}_1\psi^{(0)}_1rdr;\quad \mu_{21}=\pi\int_{L_0}F^{(2)}_1\psi^{(2)}_1rdr.$$

Table 1 facilitates interested readers by some numerical data on d_i, $\kappa^{(m)}$ and λ.

Table 1. Numerical data for computing coefficients of the modal system (1.10) versus h_1 and a. The case $h_2 = 1.0$

h_1	μ_{01}	μ_{11}	μ_{21}	$\kappa_1^{(0)}$	$\kappa_1^{(1)}$	$\kappa_1^{(2)}$	d_1	d_2	d_3	d_4	d_5	d_6	λ
Coefficients for $a = 0.4$													
0.25	1.0424	1.1096	0.4374	2.9084	0.9286	2.0076	3.6519	1.4384	0.8838	0.6474	1.7457	-0.8467	0.8971
0.30	0.9654	0.9961	0.3934	3.1778	1.0518	2.2471	2.3531	0.7392	0.8303	0.4236	1.5966	-0.5777	0.9041
0.35	0.9170	0.9140	0.3642	3.3738	1.1615	2.4383	1.6583	0.3697	0.7893	0.2839	1.4848	-0.4153	0.9095
0.40	0.8855	0.8524	0.3443	3.5136	1.2585	2.5881	1.2499	0.1569	0.7576	0.1909	1.3963	-0.3102	0.9138
0.45	0.8645	0.8048	0.3303	3.6120	1.3436	2.7038	0.9926	0.0263	0.7327	0.1262	1.3245	-0.2387	0.9170
0.50	0.8504	0.7673	0.3204	3.6805	1.4179	2.7921	0.8216	-0.0576	0.7128	0.0795	1.2656	-0.1881	0.9195
0.55	0.8408	0.7375	0.3132	3.7280	1.4822	2.8589	0.7031	-0.1135	0.6969	0.0451	1.2171	-0.1512	0.9214
0.60	0.8343	0.7134	0.3081	3.7607	1.5377	2.9091	0.6182	-0.1518	0.6839	0.0192	1.1770	-0.1235	0.9229
Coefficients for $a = 0.5$													
0.25	0.9699	0.9462	0.4106	2.9996	1.0445	2.0807	2.8393	0.9970	0.6863	0.4825	1.2082	-0.6779	0.8796
0.30	0.9199	0.8765	0.3759	3.2463	1.1588	2.3072	1.8781	0.5052	0.6965	0.3177	1.2251	-0.4677	0.8911
0.35	0.8883	0.8247	0.3526	3.4236	1.2582	2.4862	1.3578	0.2363	0.6963	0.2122	1.2223	-0.3394	0.9001
0.40	0.8674	0.7847	0.3365	3.5490	1.3445	2.6255	1.0490	0.0764	0.6916	0.1404	1.2079	-0.2556	0.9069
0.45	0.8531	0.7529	0.3251	3.6368	1.4193	2.7325	0.8527	-0.0245	0.6851	0.0893	1.1872	-0.1981	0.9121
0.50	0.8432	0.7271	0.3168	3.6978	1.4837	2.8139	0.7210	-0.0910	0.6780	0.0520	1.1642	-0.1572	0.9160
0.55	0.8362	0.7059	0.3108	3.7399	1.5391	2.8753	0.6289	-0.1363	0.6709	0.0241	1.1412	-0.1272	0.9190
0.60	0.8313	0.6885	0.3063	3.7689	1.5865	2.9214	0.5625	-0.1678	0.6644	0.0028	1.1196	-0.1047	0.9211
Coefficients for $a = 0.6$													
0.25	0.8811	0.7926	0.3721	3.1508	1.2039	2.2157	2.0178	0.5927	0.5571	0.3124	0.8822	-0.4784	0.8649
0.30	0.8639	0.7615	0.3505	3.3583	1.3024	2.4169	1.3823	0.2767	0.6014	0.2041	0.9804	-0.3360	0.8812
0.35	0.8530	0.7372	0.3356	3.5041	1.3855	2.5729	1.0363	0.0978	0.6258	0.1326	1.0365	-0.2478	0.8934
0.40	0.8450	0.7170	0.3250	3.6059	1.4560	2.6927	0.8298	-0.0120	0.6390	0.0826	1.0655	-0.1895	0.9025
0.45	0.8389	0.6999	0.3172	3.6765	1.5161	2.7839	0.6974	-0.0833	0.6454	0.0463	1.0773	-0.1490	0.9092
0.50	0.8341	0.6853	0.3113	3.7253	1.5672	2.8528	0.6079	-0.1314	0.6478	0.0192	1.0787	-0.1199	0.9141
0.55	0.8304	0.6726	0.3069	3.7589	1.6106	2.9046	0.5446	-0.1648	0.6477	-0.0013	1.0742	-0.0983	0.9177
0.60	0.8275	0.6617	0.3036	3.7819	1.6475	2.9433	0.4983	-0.1884	0.6463	-0.0170	1.0665	-0.0820	0.9203

Table 1 (continued).

h_1	μ_{01}	μ_{11}	μ_{21}	$\kappa_1^{(0)}$	$\kappa_1^{(1)}$	$\kappa_1^{(2)}$	d_1	d_2	d_3	d_4	d_5	d_6	λ
Coefficients for $a = 0.7$													
0.25	0.8049	0.6764	0.3306	3.3580	1.3991	2.4266	1.2826	0.2531	0.5073	0.1603	0.7654	-0.2876	0.8615
0.30	0.8167	0.6728	0.3228	3.5071	1.4722	2.5837	0.9303	0.0724	0.5593	0.0982	0.8780	-0.2077	0.8805
0.35	0.8233	0.6678	0.3168	3.6091	1.5321	2.7023	0.7391	-0.0331	0.5912	0.0558	0.9476	-0.1574	0.8940
0.40	0.8260	0.6619	0.3120	3.6791	1.5819	2.7918	0.6246	-0.0998	0.6107	0.0252	0.9889	-0.1235	0.9036
0.45	0.8266	0.6556	0.3081	3.7272	1.6237	2.8589	0.5504	-0.1440	0.6223	0.0026	1.0118	-0.0995	0.9104
0.50	0.8260	0.6493	0.3049	3.7603	1.6588	2.9092	0.4994	-0.1745	0.6287	-0.0146	1.0230	-0.0820	0.9153
0.55	0.8250	0.6432	0.3023	3.7829	1.6884	2.9468	0.4627	-0.1960	0.6320	-0.0277	1.0270	-0.0688	0.9187
0.60	0.8239	0.6375	0.3003	3.7984	1.7133	2.9747	0.4354	-0.2113	0.6333	-0.0379	1.0268	-0.0588	0.9211
Coefficients for $a = 0.8$													
0.25	0.7736	0.6156	0.3003	3.5858	1.5991	2.6972	0.7201	-0.0148	0.5271	0.0401	0.8083	-0.1391	0.8777
0.30	0.7977	0.6235	0.3020	3.6648	1.6403	2.7901	0.5846	-0.0965	0.5674	0.0111	0.8909	-0.1061	0.8936
0.35	0.8107	0.6267	0.3021	3.7180	1.6738	2.8585	0.5108	-0.1457	0.5923	-0.0095	0.9413	-0.0845	0.9042
0.40	0.8172	0.6271	0.3013	3.7541	1.7015	2.9092	0.4653	-0.1776	0.6075	-0.0246	0.9712	-0.0694	0.9113
0.45	0.8201	0.6260	0.3001	3.7787	1.7245	2.9469	0.4347	-0.1993	0.6167	-0.0361	0.9883	-0.0584	0.9162
0.50	0.8212	0.6240	0.2990	3.7955	1.7438	2.9748	0.4126	-0.2144	0.6220	-0.0448	0.9974	-0.0502	0.9195
0.55	0.8215	0.6217	0.2979	3.8070	1.7599	2.9956	0.3962	-0.2253	0.6250	-0.0515	1.0016	-0.0438	0.9217
0.60	0.8214	0.6193	0.2970	3.8149	1.7733	3.0109	0.3835	-0.2331	0.6265	-0.0567	1.0029	-0.0389	0.9233
Coefficients for $a = 0.9$													
0.25	0.7959	0.6069	0.2917	3.7647	1.7496	2.9470	0.4195	-0.1917	0.5901	-0.0400	0.9328	-0.0532	0.9090
0.30	0.8086	0.6106	0.2942	3.7862	1.7650	2.9753	0.3976	-0.2116	0.6052	-0.0486	0.9609	-0.0453	0.9153
0.35	0.8148	0.6119	0.2952	3.8007	1.7777	2.9960	0.3834	-0.2244	0.6139	-0.0550	0.9766	-0.0396	0.9192
0.40	0.8179	0.6119	0.2954	3.8106	1.7883	3.0113	0.3730	-0.2331	0.6189	-0.0597	0.9851	-0.0353	0.9217
0.45	0.8193	0.6113	0.2953	3.8173	1.7971	3.0225	0.3651	-0.2392	0.6217	-0.0634	0.9895	-0.0320	0.9234
0.50	0.8199	0.6104	0.2951	3.8219	1.8045	3.0309	0.3589	-0.2436	0.6233	-0.0662	0.9915	-0.0294	0.9245
0.55	0.8201	0.6094	0.2949	3.8250	1.8106	3.0370	0.3539	-0.2467	0.6241	-0.0684	0.9921	-0.0273	0.9252
0.60	0.8202	0.6084	0.2947	3.8271	1.8157	3.0415	0.3499	-0.2490	0.6244	-0.0701	0.9919	-0.0257	0.9257

Table 2. Convergence of d_1 and d_2 versus I_0 in the Fourier series (1.14) ($a = 0.7$; $h_2 = 0.5$).

	$h_1 = 0.3$		$h_1 = 0.5$	
I_0	d_1	d_2	d_1	$-d_2$
1	0.91465	0.064550	0.52435	0.16810
2	1.00504	0.095611	0.53062	0.16729
3	1.01616	0.099171	0.53091	0.16729
4	1.01640	0.099204	0.53093	0.16728
5	1.01645	0.099239	0.53094	0.16728
6	1.01647	0.099245	0.53094	0.16728

The integrals above contain several relatively complex expressions that were denoted as

$$\mathcal{G}_1 = \frac{\partial F_1^{(1)}}{\partial r}\frac{\partial \psi_1^{(1)}}{\partial r} - F_1^{(1)}\frac{\partial^2 \psi_1^{(1)}}{\partial z^2}; \quad \mathcal{G}_2 = \frac{1}{r^2}F_1^{(1)}\psi_1^{(1)},$$

$$\mathcal{G}_3 = \frac{1}{2}\left[\frac{\partial}{\partial r}\left((F_1^{(1)})^2\frac{\partial^2 \psi_1^{(1)}}{\partial z \partial r}\right) + \frac{(F_1^{(1)})^2}{r}\frac{\partial^2 \psi_1^{(1)}}{\partial z \partial r} - \frac{\partial \psi_1^{(1)}}{\partial z}\frac{(F_1^{(1)})^2}{r^2}\right],$$

$$\mathcal{G}_5 = \frac{\partial}{\partial r}\left(F_1^{(1)}\frac{\partial \Psi_0}{\partial r} + \frac{F_1^{(1)}}{r}\frac{\partial \Psi_0}{\partial r}\right); \quad \mathcal{G}_7 = \frac{2F_1^{(1)}}{r^2}\Psi_2,$$

$$\mathcal{G}_6 = \frac{\partial}{\partial r}\left(F_1^{(1)}\frac{\partial \Psi_2}{\partial r}\right) + \frac{F_1^{(1)}}{r}\frac{\partial \Psi_2}{\partial r} - 4\frac{F_1^{(1)}}{r^2}\Psi_2,$$

$$\mathcal{G}_{01} = \frac{\partial F_1^{(0)}}{\partial r}\frac{\partial \psi_1^{(1)}}{\partial r} - F_1^{(0)}\frac{\partial^2 \psi_1^{(1)}}{\partial z^2}; \quad \mathcal{G}_{12} = \frac{\partial F_1^{(1)}}{\partial r}\frac{\partial \psi_1^{(2)}}{\partial r} - F_1^{(1)}\left(\frac{\partial^2 \psi_1^{(2)}}{\partial z^2} - \frac{2}{r^2}\psi_1^{(2)}\right),$$

$$\mathcal{G}_{21} = \frac{\partial F_1^{(2)}}{\partial r}\frac{\partial \psi_1^{(1)}}{\partial r} + F_1^{(2)}\left(\frac{1}{r^2}\psi_1^{(1)} - \frac{\partial^2 \psi_1^{(1)}}{\partial z^2}\right).$$

The last expressions include the functions $\Psi_0(z,r)$ and $\Psi_2(z,r)$ which are solutions of the Neumann boundary value problems in the meridional plane G:

$$\begin{aligned} &L_0(\Psi_0) = 0 \quad \text{in } G; \quad |\Psi_0(0,z)| < \infty, \\ &\frac{\partial \Psi_0}{\partial \nu} = 0 \quad \text{on } L_1; \quad \frac{\partial \Psi_0}{\partial \nu} = \frac{1}{2}(\mathcal{G}_1 + \mathcal{G}_2) \quad \text{on } L_0; \end{aligned} \tag{1.12}$$

and

$$\begin{aligned} &L_2(\Psi_2) = 0 \quad \text{in } G; \quad |\Psi_2(0,z)| < \infty, \\ &\frac{\partial \Psi_2}{\partial \nu} = 0 \quad \text{on } L_1; \quad \frac{\partial \Psi_2}{\partial \nu} = \frac{1}{2}(\mathcal{G}_1 - \mathcal{G}_2) \quad \text{on } L_0. \end{aligned} \tag{1.13}$$

These solutions were found in terms of Fourier series based on fundamental linear solutions, i.e.

$$\Psi_0 = \lim_{I_0 \to \infty} \sum_{i=1}^{I_0} a_i \psi_i^{(0)}(z,r), \quad \Psi_2 = \lim_{I_0 \to \infty} \sum_{i=1}^{I_0} b_i \psi_i^{(2)}(z,r), \tag{1.14}$$

where

$$a_i = \frac{\int_{L_0}(\mathcal{G}_1+\mathcal{G}_2)\psi_i^{(0)}rdr}{2\kappa_i^{(0)}\int_{L_0} r(\psi_i^{(0)})^2dr}; \quad b_i = \frac{\int_{L_0}(\mathcal{G}_1-\mathcal{G}_2)\psi_i^{(2)}rdr}{2\kappa_i^{(2)}\int_{L_0} r(\psi_i^{(2)})^2dr}.$$

These Fourier approximations are quite efficient and guarantee prompt convergence to d_1 and d_2. The convergence in (1.14) versus I_0 is illustrated in Table 2.

There are several limitations in implementing the modal modelling, in general, and the modal system (1.10), in particular. A natural limitation is associated with numerical-analytical method of Part 1, which is numerically stable only for $h_1 \geq 0.1$ and $a \geq 0.3$. Later on, since $h_1 = 0.1$ is quite small to disable baffle's sloping in nonlinear wave regimes and, even if this does not happen, causes shallow fluid flows over the baffle, the limitation on h_1 should be stronger. Using an estimate of the shallow water phenomena by Miles [28], we restrict ourselves to $h_1 \geq 0.2$.

In addition, limitation on a must be stronger due to numerical difficulties. In fact, computing d_i needs higher derivatives of $\psi_i^{(m)}(r,z)\begin{matrix}\cos\\ \sin\end{matrix}\eta$, but the methods of Part 1 showed good convergence of these higher derivatives only for $a \geq 0.38$. Finally, we will consider only $h_1 + h_2 \geq 1$, namely, only fairly deep fluid fillings.

2. Steady-state resonant waves

2.1. Galerkin scheme

When considering harmonic horizontal forcing (1.2) in the modal system (1.10) and accounting for the asymptotic relationships (1.8) we pose dominating modal functions as

$$\beta^c_{1,1}(t) = A\cos\sigma t + \bar{A}\sin\sigma t + o(\epsilon^{1/3}),\ \beta^s_{1,1}(t) = \bar{B}\cos\sigma t + B\sin\sigma t + o(\epsilon^{1/3}). \tag{2.1}$$

Setting (2.1) in (1.10c)-(1.10e) and using the Fredholm alternative give

$$\begin{aligned}
\beta^c_{0,1}(t) &= c_0 + c_1\cos 2\sigma t + c_2\sin 2\sigma t + o(\epsilon^{2/3}),\\
\beta^c_{2,1}(t) &= s_0 + s_1\cos 2\sigma t + s_2\sin 2\sigma t + o(\epsilon^{2/3}),\\
\beta^s_{2,1}(t) &= e_0 + e_1\cos 2\sigma t + e_2\sin 2\sigma t + o(\epsilon^{2/3}),
\end{aligned} \tag{2.2}$$

where

$$\begin{aligned}
&c_0 = l_0(A^2+\bar{A}^2+B^2+\bar{B}^2);\quad c_1 = p_0(A^2-\bar{A}^2-B^2+\bar{B}^2),\\
&c_2 = 2p_0(A\bar{A}+B\bar{B});\quad s_0 = l_2(A^2+\bar{A}^2-B^2-\bar{B}^2),\\
&s_1 = p_2(A^2-\bar{A}^2+B^2-\bar{B}^2);\quad s_2 = 2p_2(A\bar{A}-B\bar{B}),\\
&e_0 = -2l_2(A\bar{B}+B\bar{A});\quad e_1 = 2p_2(\bar{A}B-A\bar{B});\quad e_2 = -2p_2(AB+\bar{A}\bar{B})
\end{aligned} \tag{2.3}$$

and

$$\begin{aligned}
&p_0 = \frac{D_{10}+D_8}{2(\bar{\sigma}_0^2-4)},\quad l_0 = \frac{D_{10}-D_8}{2\bar{\sigma}_0^2},\\
&p_2 = \frac{D_9+D_7}{2(\bar{\sigma}_2^2-4)},\ l_2 = \frac{D_9-D_7}{2\bar{\sigma}_2^2};\quad \bar{\sigma}_m = \frac{\omega_1^{(m)}}{\sigma},\ m = 0,1,2.
\end{aligned} \tag{2.4}$$

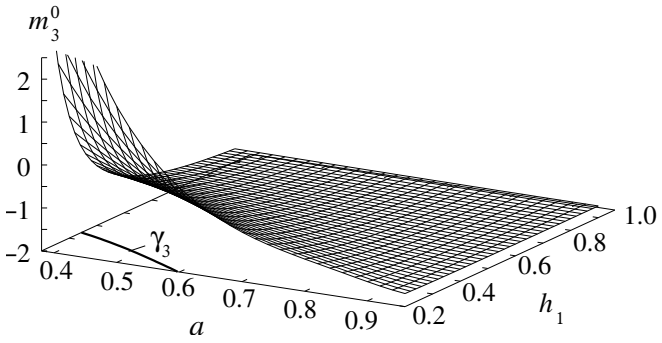

Fig. 3. $m_3^{(0)}$ versus (h_1, a) for $h_1 + h_2 = 1$.

By substituting (2.1) and (2.2) into (1.10a)-(1.10b) and using the Fredholm alternative we get the following system of algebraic equations of the four unknown variables $A, \bar{A}, B, \bar{B}$

$$\begin{aligned}
&A[\bar{\sigma}_1^2 - 1 + m_1(A^2 + \bar{A}^2 + \bar{B}^2) + m_2 B^2] + m_3 \bar{A} B \bar{B} = \Lambda\epsilon,\\
&\bar{A}[\bar{\sigma}_1^2 - 1 + m_1(A^2 + \bar{A}^2 + B^2) + m_2 \bar{B}^2] + m_3 A B \bar{B} = 0,\\
&B[\bar{\sigma}_1^2 - 1 + m_1(B^2 + \bar{A}^2 + \bar{B}^2) + m_2 A^2] + m_3 \bar{B} A \bar{A} = 0,\\
&\bar{B}[\bar{\sigma}_1^2 - 1 + m_1(A^2 + B^2 + \bar{B}^2) + m_2 \bar{A}^2] + m_3 \bar{A} A B = 0,
\end{aligned} \tag{2.5}$$

where

$$\begin{aligned}
m_1 &= D_5(\tfrac{1}{2}p_0 - l_0) - D_3(\tfrac{1}{2}p_2 - l_2) - 2D_6 p_0 - 2D_4 p_2 - \tfrac{1}{2}D_1,\\
m_2 &= -D_3(l_2 + \tfrac{3}{2}p_2) - D_5(l_0 + \tfrac{1}{2}p_0) + 2D_6 p_0 - 6D_4 p_2 + \tfrac{1}{2}D_1 - 2D_2,\\
m_3 &= m_1 - m_2
\end{aligned} \tag{2.6}$$

are functions of σ, h_1, h_2 and a.

Accounting for the resonance condition $\bar{\sigma}_1 \to 1$ and $A \sim \bar{A} \sim B \sim \bar{B} = O(\epsilon^{1/3})$ one deduces that

$$\bar{\sigma}_1^2 - 1 = O(\epsilon^{2/3}); \quad m_i(\sigma, h_1, h_2, a) = m_i^0(h_1, h_2, a) + o(\epsilon^{1/3}), \quad i = 1, 2, 3, \tag{2.7}$$

where the first relationship implies the so-called Moiseyev asymptotic detuning and $m_i^0 = m_i(\omega_1^{(1)}, h_1, h_2, a) = O(1)$ (computing m_i^0 means setting $\sigma \equiv \omega_1^{(1)}$ in (2.4)).

When analysing similar algebraic systems, Gavrilyuk *et al.* [18] and Faltinsen *et al.* [15] showed that resolvability condition for (2.5) is

$$A \neq 0; \quad \bar{A} = 0; \quad m_3^0 \neq 0. \tag{2.8}$$

Neglecting $o(\epsilon)$ in (2.5) one re-writes the system to the following form

$$A(\bar{\sigma}_1^2 - 1 - m_1^0 A^2 - m_2^0 B^2) = \epsilon\Lambda, \quad B(\bar{\sigma}_1^2 - 1 - m_1^0 B^2 - m_2^0 A^2) = 0, \quad \bar{A} = \bar{B} = 0. \tag{2.9}$$

The features of (2.9) are then predetermined by the geometric triad (h_1, h_2, a), but its

solutions (A, B) change with $\bar{\sigma}_1$. By fixing the fluid fill level $H = h_1 + h_2$, the coefficient m_3^0 can be evaluated as a function of h_1 and a. Calculation showed that the zeros of m_3^0 lay on the curve γ_3 in the (a, h_1)-plane as demonstrated in Figure 3 for $H = 1$. We have found that γ_3 is almost invariant for larger $H \geq 1$.

2.2. Steady-state wave regimes

Taking into account the resolvability condition (2.8) and repeating the analysis by Lukovsky [24] and Faltinsen *et al.* [10] we find that there exist only two possible solutions of (2.9). They correspond to
(i) 'planar' wave regime

$$f(r, \eta, t) = AF_1^{(1)}(r) \cos\eta \cos\sigma t + o(\epsilon^{1/3}) \tag{2.10}$$

occurring for $B = 0$ and
(ii) 'swirling' wave regimes

$$f(r, \eta, t) = F_1^{(1)}(r)(A \cos\eta \cos\sigma t \pm B \sin\eta \sin\sigma t) + o(\epsilon^{1/3}) \tag{2.11}$$

occurring for $B \neq 0$. The $\pm$ ahead of amplitude component B in (2.11) means two solutions which determine either clockwise or counterclockwise rotary wave. Since both signs are mathematically possible, initial conditions and transient phase should determine the sign.

2.3. Stability

Stability of the steady-state solutions (2.10) and (2.11) can be studied by combining the first Lyapunov method and the multi-timing technique (see, Miles [29] and Faltinsen *et al.* [10]). This introduces the slowly varying time $\tau = \epsilon^{2/3}\sigma t/2$ and

$$\begin{aligned} \beta_{1,1}^c &= (A + \alpha(\tau)) \cos\sigma t + \bar{\alpha}(\tau) \sin\sigma t + o(\epsilon^{1/3}), \\ \beta_{1,1}^s &= \bar{\beta}(\tau) \cos\sigma t + (B + \beta(\tau)) \sin\sigma t + o(\epsilon^{1/3}), \end{aligned} \tag{2.12}$$

where $\alpha, \bar{\alpha}, \beta$ and $\bar{\beta}$ are infinitesimal perturbations varying with τ and A and B are solutions of (2.9).

Gathering terms of the lowest asymptotic order and keeping linear terms in $\alpha, \bar{\alpha}, \beta$ and $\bar{\beta}$ lead to the following linear system of ordinary differential equations

$$\mathbf{c}' + [\delta\mathbf{c}] + \mathcal{C}\mathbf{c} = 0, \tag{2.13}$$

where a speculative small damping rate $\delta > 0$ is incorporated.

Further, $\mathbf{c} = (\alpha, \bar{\alpha}, \beta, \bar{\beta})^T$ and the matrix $\mathcal{C}$ has the following non-zero elements

$$\begin{aligned} &c_{12} = -[\bar{\sigma}_1^2 - 1 + m_1^0 A^2 + m_1^0 B^2]; \quad c_{21} = \bar{\sigma}_1^2 - 1 + 3m_1^0 A^2 + m_2^0 B^2, \\ &c_{14} = -(m_1^0 - m_2^0)AB; \quad c_{41} = -2m_2^0 AB, \\ &c_{23} = 2ABm_2^0; \quad c_{32} = (m_1^0 - m_2^0)AB, \\ &c_{34} = \bar{\sigma}_1^2 - 1 + m_1^0 B^2 + m_1^0 A^2; \quad c_{43} = -[\bar{\sigma}_1^2 - 1 + 3m_1^0 B^2 + m_2^0 A^2]. \end{aligned}$$

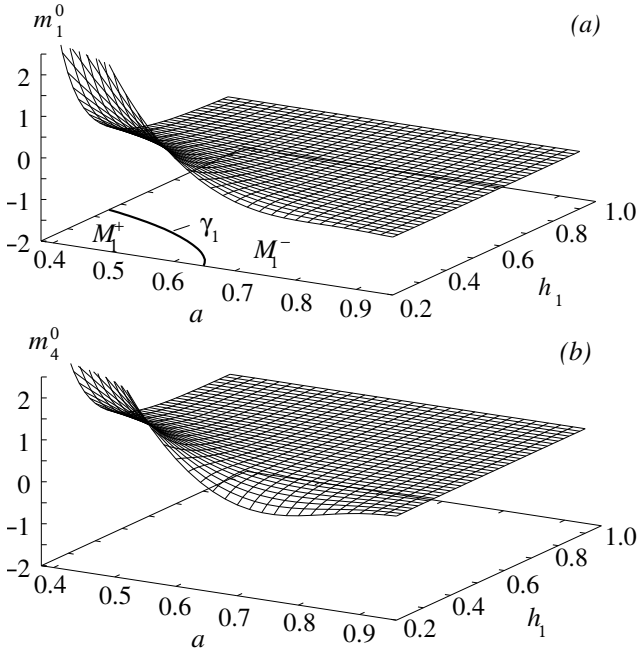

Fig. 4. $m_1^{(0)}$ and $m_4^{(0)}$ versus a and h_1 for $h_1 + h_2 = 1$.

Fundamental solutions of (2.13) depend on the eigenvalue problem $\det[(\lambda+\delta)E+C] = 0$. Computations give the following characteristic polynomial

$$(\lambda + \delta)^4 + c_1(\lambda + \delta)^2 + c_0 = 0, \tag{2.14}$$

where c_0 is the determinant of $\mathcal{C}$ and c_1 is a complicated function of the elements of $\mathcal{C}$. Since the eigenvalues λ can be expressed as $-\delta \pm \sqrt{x_{1,2}}$ ($x_{1,2}$ are solutions of the equation $x^2 + c_1 x + c_0 = 0$), the asymptotic stability of the fixed point solutions means that

$$c_0 > 0; \quad c_1 > 0; \quad c_1^2 - 4c_1 > 0. \tag{2.15}$$

Here c_0 vanishes at the turning point solutions and at Poincare-bifurcation points. The zeros of the discriminant $c_1^2 - 4c_1$ are Hopf-bifurcation points where the real parts of a pair of complex-conjugate zeros of c_0 becomes positive.

The analysis of the next section will be done for $\delta = 0$. One should note, that small positive δ do not lead to instability of a steady-state regime, but rather can reduce frequency domains where such regimes are unstable.

2.4. Response curves of 'planar' and 'swirling' regimes versus h_1 and a

The dominating amplitude A of 'planar' wave regime (i) is governed by the single equation

$$A(\bar{\sigma}_1^2 - 1 + m_1^0 A^2) = \Lambda\epsilon; \quad B = 0, \tag{2.16}$$

but the pair (A, B) of (ii), which describes 'swirling', should be found from the algebraic equation

$$A(\bar{\sigma}_1^2 - 1 + m_4^0 A^2) = m_5 \Lambda \epsilon, \quad m_5^0 = -\frac{m_1^0}{m_3^0}, \quad m_4^0 = m_1^0 + m_2^0 \tag{2.17}$$

and the auxiliary formula for computing B

$$B^2 = \frac{1}{m_1^0}(\bar{\sigma}_1^2 - 1 + m_2^0 A^2) > 0, \tag{2.18}$$

where A is solution of (2.17).

Existence and properties of (i) and (ii) depend on solutions of the cubic equations (2.16) and (2.17) and, as a consequence, on the signs of m_1^0 and m_4^0 (Miles [28], Gavrilyuk *et al.* [18] and Faltinsen *et al.* [10]). If $h_1 + h_2 \geq 1$ and $a \geq 0.38, h_1 > 0.2$, numerical testing finds $m_4^0 > 0$, but m_1^0 changes its sign on a curve γ_1 in the (a, h_1)-plane. This point is illustrated in Figure 4, where M_1^+ and M_1^- are areas of positive and negative m_1^0, respectively.

Analysis in Figures 5 (a-e) for $\epsilon = 0.002, h_1 + h_2 = 1$ and $h_1 = 0.3$ displays evolution of the response curves with decreasing $a \leq 1$ (baffle is introduced deeper into the fluid bulk for each new figure). The value $h_1 = 0.3$ guarantee that the pairs (a, h_1) runs from M_1^- to M_1^+ and, therefore, effect of changing 'soft-spring' to 'hard-spring' behaviour at γ_1 is captured.

In Figures 5 (a-e), we treat A and B as (dominating) amplitudes of longitudinal (along oscillations of the tank) and transversal (perpendicular to the oscillations) wave elevations in steady-state wave regimes. Since A and B are functions of $1/\bar{\sigma}_1$, the response curves are considered in the $(1/\bar{\sigma}_1, |A|, |B|)$-space. Their projections on the $(1/\bar{\sigma}_1, |A|)$-plane express solutions of (2.16) and (2.17). Figures 5 (a-e) represent both these projections and three-dimensional views. Solid lines are used for stable solutions, but dashed lines denote unstable solutions.

Figure 5 (a) starts with the case of smooth circular cylindrical tank (there is no baffle). The branching of this figure has been established by Miles [28, 29], Lukovsky [24], Lukovsky & Timokha [25] and Gavrilyuk *et al.* [18]. The analysis gives the turning point T for 'planar' response curve, the Poincare-bifurcation point P, where 'planar' response curve bifurcates to 'swirling' (this fact is demonstrated by three-dimensional view) and H is the Hopf-bifurcation point, where 'swirling' changes its stability properties. In order to classify the wave regimes versus $1/\bar{\sigma}_1$ the frequency domains of stable 'planar' and 'swirling' solutions are incorporated in the $(1/\bar{\sigma}_1, |A|)$-plane. These domains show zones where the corresponding wave regimes exist, stable and have minimum energy with respect to other stable steady-state waves. In addition, we denoted as 'chaotic' the frequency domain, where our analysis did not find any stable steady-state waves and, therefore, we expect chaotic motions.

In Figure 5 (b), we show that a narrow ring baffle ($a = 0.7$) does not change shapes of the branches. There is a small drift of 'chaotic' frequency domain, but its range (interval between abscissas of T and H) is almost unchanged. A migration of 'chaotic' frequency domain becomes visible only if $(a, h_1) \in M_1^-$ approaches to γ_1. The situation is depicted in Figure 5 (c), which is drawn for $a = 0.6$. Here, m_1^0 is close to zero and, therefore, response curves responsible for 'planar' regimes (found from (2.16)) are approximately the same as in the linear sloshing theory. The Hopf-bifurcation point H moves to the right and projections

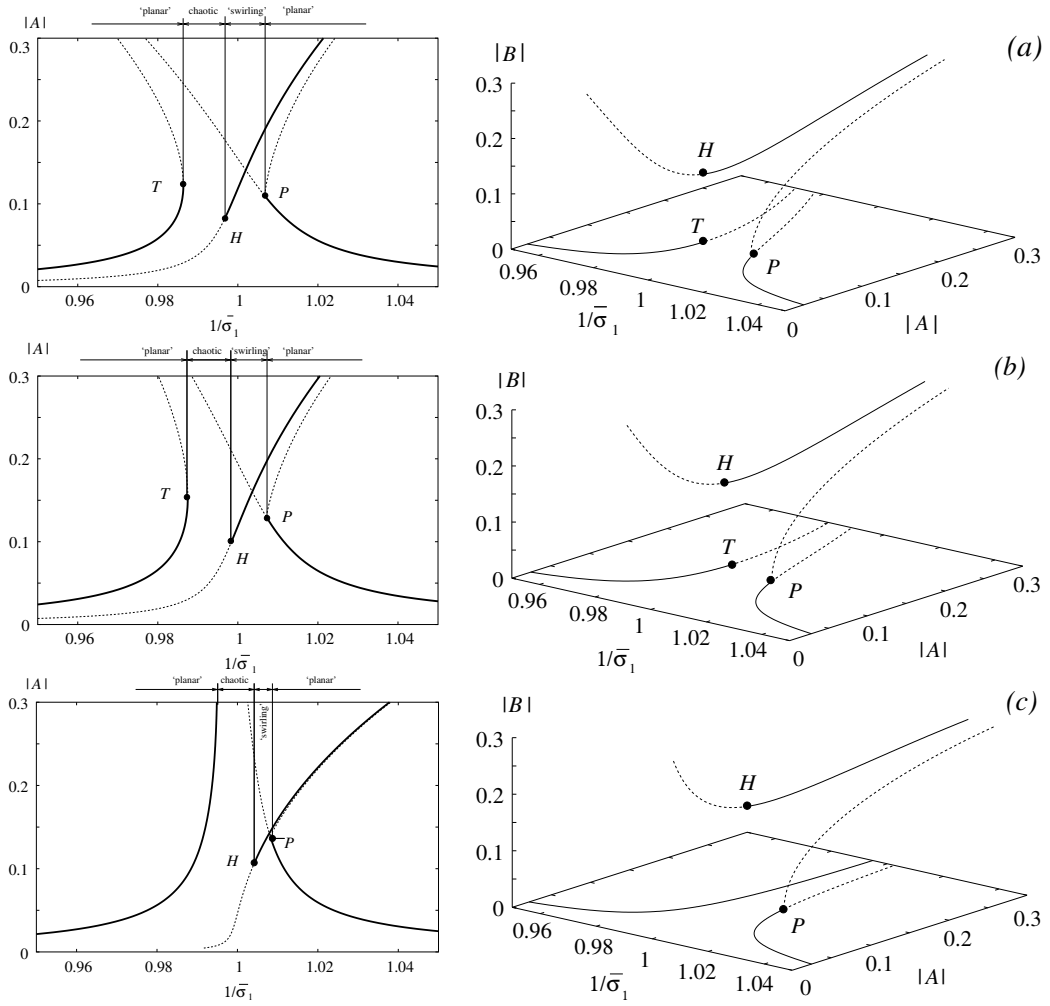

Fig. 5. Response curves for $\epsilon = 0.002, h_1 + h_2 = 1$ and $h_1 = 0.3$. Each row gives $|A|$ versus $1/\bar{\sigma}_1$ in the $(1/\bar{\sigma}_1, |A|)$-plane and spatial representation of the triads $(1/\bar{\sigma}_1, |A|, |B|)$. A implies longitudinal wave component (in the forcing plane) and B notes transversal component (perpendicular to the forcing). The solid lines correspond to stable solutions and the dashed lines are used for unstable steady-state wave regimes. We present the effective frequency domains for 'planar' and 'swirling' solutions. 'Chaotic' domain marks the absence of stable steady-state regimes. (a) The tank has no baffle ($a = 1$); T is the turning point of 'planar' regime, P is the Poincare-bifurcation point, where unstable 'swirling' appears from 'planar' solutions and H is the Hopf-bifurcation point. (b) corresponds to $a = 0.7$; bifurcation points are as in the case (a). (c) The same as in (b), but for $a = 0.6$.

of 'swirling' curves on the $(1/\bar{\sigma}_1, |A|)$-axis become close to each other. That is why, the three-dimensional representation is this case more informative.

When (a, h_1) runs into M_1^+, the branching of response curves changes dramatically. Examples are given in Figures 5 (d,e) for $a = 0.5$ and 0.4. First of all, we find out that earlier bifurcation points disappear. Besides, frequency domain of 'chaotic' motions is removed at

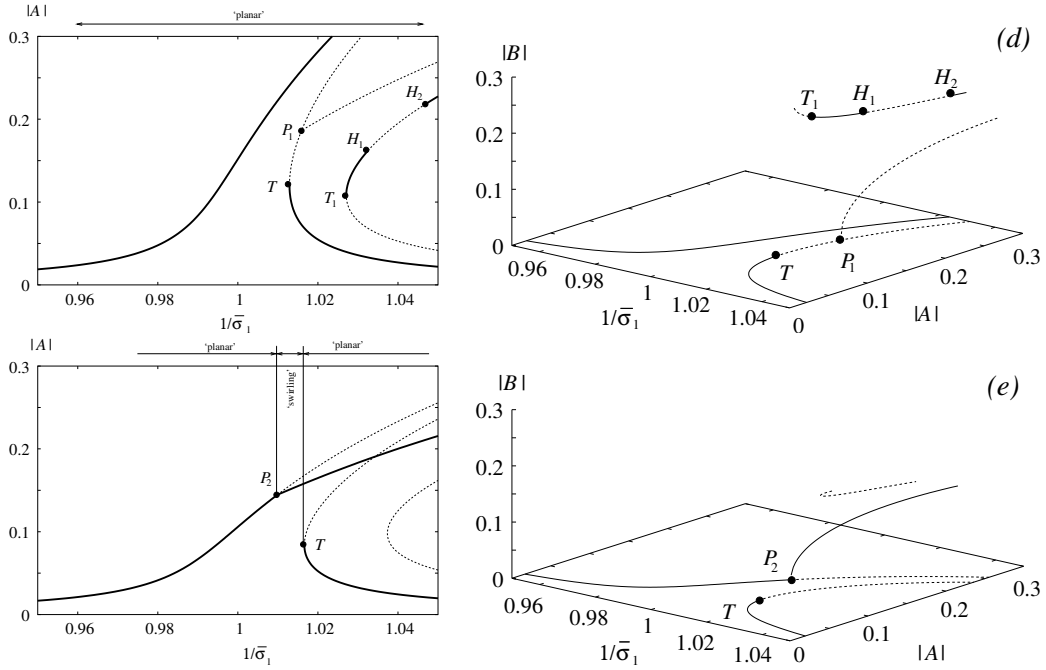

Fig. 5 (continued). (d) represents the branching for $a = 0.5$; T is the turning point for 'planar' solutions, P_1 implies the Poincare-bifurcation point, where both regimes are unstable, T_1 is the turning point for 'swirling' and H_i, $i = 1, 2$ are the Hopf-bifurcation points. (e) gives the results for $a = 0.4$; T is the turning point for 'planar' response curve and P_2 is the Poincare-bifurcation point.

all as well as response curves responsible for 'swirling' move away from the primary resonance $1/\bar{\sigma}_1 = 1$. In the case $a = 0.5$ depicted in Figure 5 (d), 'planar' solution is stable in all the resonant frequency domain and 'swirling' does not realise (stable 'swirling' between the turning point T_1 and the Hopf-bifurcation point H_1 and in a zone in the right of H_2 correspond to waves of higher kinetic energy than corresponding 'planar' regime). Figure 5 (e) shows that T_1, H_1 and H_2-bifurcation points disappear with decreasing a to 0.4 and the Poincare-bifurcation point P_1 "jumps" to P_2, i.e. from one 'planar' branch to another. In addition, there is a frequency domain, where our theory expects stable 'swirling', but unstable 'planar' waves.

One should note, that non-zero damping $\delta > 0$ from § 2.3 can increase effective frequency domains of stable steady-state solutions and zone of 'chaotic' waves may disappear for $(a, h_1) \in M_1^-$, but the qualitative conclusion on the effective frequency domains should be the same. we do not present suitable analysis, because we are sure that effect of damping on resonant baffled sloshing should account for realistic dissipation rates due to shear stress (Hill [20]) and vorticity stress at the baffle edge (Buzhinskii [3]). This consititite an interesting perspective for future work and will be of special attention in the forthcoming paper.

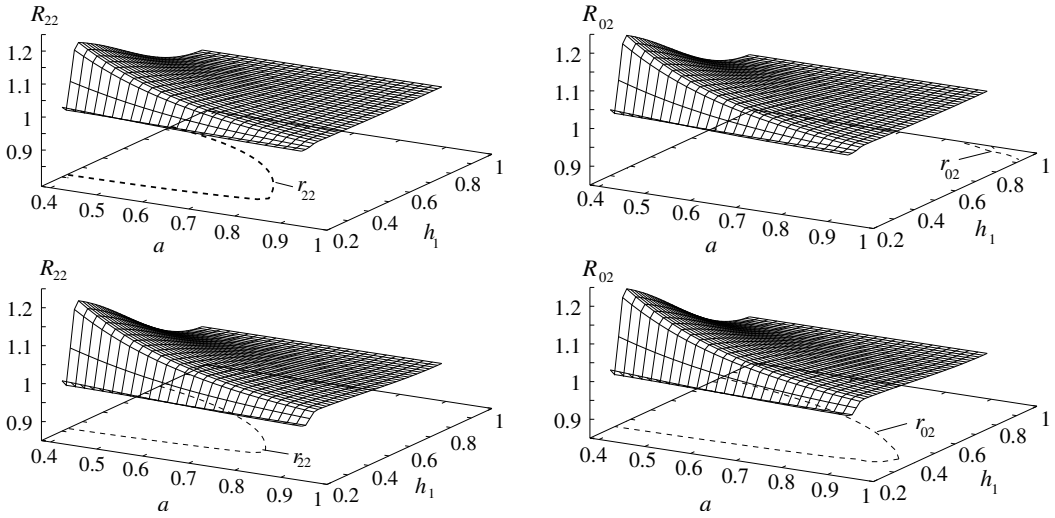

Fig. 6. R_{22} and R_{02} for $h_1 + h_2 = 1$ (first row) and for $h_1 + h_2 = 2$ (second row). Contours r_{22} and r_{02} represent solutions of the equations $R_{22}(a, h_1) = 1$ and $R_{02}(a, h_1) = 1$, respectively.

3. Secondary resonance as a perspective direction

Another interesting perspective consists of increasing the dimension of the modal system. This operation is of importance when the secondary resonance phenomena cause amplification of $\beta^c_{2,i}$, $\beta^s_{2,i}$, $\beta^c_{0,i}$, $\beta^s_{0,i}$, $i \geq 2$ and (1.9) fails. Miles [28] showed that the latter occurs in circular basin near a depth to radius ratio 0.831, when the first harmonic of wave progressing around the basin forces resonantly the second harmonic of the wave causing the two harmonics to be of comparable magnitude. A resonance triad is set up consisting of the first harmonic interacting with itself and the second harmonic.

The internal resonances are discussed by Bryant [2] (circular basin), these are extensively examined for large amplitude forcing by Faltinsen & Timokha [14, 15] (rectangular tank), Ockendon *et al.* [33], La Rocca *et al.* [22, 23] and Faltinsen *et al.* [10] (square base tank). Following Bryant [2] we expect those internal resonances when one from

$$R_{0i} = \frac{1}{2}\sqrt{\frac{\kappa_{0i}}{\kappa_{11}}}; R_{2i} = \frac{1}{2}\sqrt{\frac{\kappa_{2i}}{\kappa_{11}}},\ i \geq 1 \tag{3.1}$$

passes to 1. Our numerical analysis showed that only R_{22} and R_{02} can be equal to 1. Figure 6 illustrates the curves r_{22} and r_{02} on which the secondary resonance occurs.

References

[1] BOGORYAD, I.B. & DRUZHININA, G.Z.: 1985 On the damping of sloshing a viscous fluid in cylindrical tank with annular baffle. *Soviet Applied Mechanics.* **21**, N 2, 126-128

[2] BRYANT, P.J. 1989 Nonlinear progressive waves in a circular basin. *J. Fluid Mech.* **205**, 453-467.

[3] BUZHINSKII, V.A.: 1998 Vortex damping of sloshing in tanks with baffles. *J. Appl. Maths. Mechs.* **62**, N 2, 217-224.

[4] CARIOU, A.& CASELLA, G.: 1999 Liquid sloshing in ship tanks: a comparative study of numerical simulation. *Marine Structure*, **12**, 183-198.

[5] CELEBI, S.M.& AKYILDIZ, H.: 2002 Nonlinear modelling of liquid sloshing in a moving rectangular tank. *Ocean Engineering.* **29**, 1527-1553.

[6] CHO, J.R.& LEE, H.W.: 2003 Dynamic analysis of baffled liquid-storage tanks by the structural-acoustic finite element formulation. *Journal Sound and Vibration*, **258(5)**, 847-866.

[7] CHO, J.R.& LEE, H.W.: 2004 Numerical study on liquid sloshing in baffled tank by nonlinear finite element method. *Comput. Methods Appl. Mech. Engrg.* **193**, 2581-2598.

[8] CHO, J.R.& LEE, H.W.: 2004 Non-linear finite element analysis of large amplitude sloshing flow in two-dimensional tank. *Int. J. Num. Methods in Engineering.* **61**, 514-531.

[9] COLAGROSSI A, LANDRINI M.: 2003 Numerical simulation of interfacial flows by smoothed particle hydrodynamics. *J. Comput. Phys.*,**191** N 2, 448-475.

[10] FALTINSEN, O.M., ROGNEBAKKE, O.F.& TIMOKHA, A.N.: 2003 Resonant three-dimensional nonlinear sloshing in a square base basin. *Journal of Fluid Mechanics*, **487**, 1-42.

[11] FALTINSEN, O.M., ROGNEBAKKE, O.F. & TIMOKHA, A.N.: 2005 Resonant three-dimensional nonlinear sloshing in a square base basin. Part 2. Effect of higher modes. *J. Fluid Mech.* **523**, 199-218.

[12] FALTINSEN, O.M., ROGNEBAKKE, O.F.& TIMOKHA, A.N.: 2005 Classification of three-dimensional nonlinear sloshing in a square-base tank with finite depth. *Journal of Fluids and Structures*, **20**, N 1, 81-103.

[13] FALTINSEN, O.M., ROGNEBAKKE, O.F., LUKOVSKY, I.A.& TIMOKHA, A.N.: 2000 Multidimensional modal analysis of nonlinear sloshing in a rectangular tank with finite water depth. *Journal of Fluid Mechanics*, **407**, 201–234.

[14] FALTINSEN, O.M.& TIMOKHA, A.N. 2001 Adaptive multimodal approach to nonlinear sloshing in a rectangular rank. *J. Fluid Mech.* **432**, 167-200.

[15] FALTINSEN, O.M.& TIMOKHA, A.N.: 2002 Asymptotic modal approximation of nonlinear resonant sloshing in a rectangular tank with small fluid depth. *J. Fluid Mech.* **470**, 319-357.

[16] FALTINSEN, O.M.& TIMOKHA, A.N. 2002b Analytically-oriented approaches to two-dimensional fluid sloshing in a rectangular tank (survey). *Proceedings of the Institute of Mathematics of the Ukrainian National Academy of Sciences: "Problems of Analytical Mechanics and its Applications".* **44**, 321-345.

[17] FESCHENKO, S.F., LUKOVSKY, I.A., RABINOVICH, B.I.& DOKUCHAEV, L.V.: 1969. The methods for determining the added fluid masses in mobile cavities. *Naukova dumka, Kiev* (in Russian).

[18] GAVRILYUK, I., LUKOVSKY, I.A. & TIMOKHA, A.N.: 2000. A multimodal approach to nonlinear sloshing in a circular cylindrical tank. *Hybrid Methods in Engineering*, **2**, N 4, 463-483.

[19] GAVRILYUK, I., LUKOVSKY, I.A., TROTSENKO, YU.& TIMOKHA, A.N.: 2005 The fluid sloshing in a vertical circular cylindrical tank with a rigid-ring baffle I: Linear fundamental solutions. *J. Engr. Math.* to appear.

[20] HILL, D.H.: 2003 Transient and steady-state amplitudes of forced waves in rectangular tanks. *Physics of Fluids*, **15**, N 6, 1576-1587.

[21] IBRAHIM, R.A., PILIPCHUK, V.N.& IKEDA, T.: 2001 Recent advances in liquid sloshing dynamics. *Applied Mechanics Research,* **54(2)**, 133-199.

[22] LA ROCCA, M., MELE, P.& ARMENIO, V.: 1997 Variational approach to the problem of sloshing in a moving container. *Journal of Theoretical and Applied Fluid Mechanics*, **1**, N 4, 280-310.

[23] LA ROCCA, M., SCIORTINO, G.& BONIFORTI, M.A.: 2000. A fully nonlinear model for sloshing in a rotating container. *Fluid Dynamics Research*, **27**, 23-52.

[24] LUKOVSKY, I.A.: 1990 Introduction to the nonlinear dynamics of a limited liquid volume. *Naukova Dumka, Kiev* (in Russian).

[25] LUKOVSKY, I.A., TIMOKHA, A.N.: 1995 Variational methods in nonlinear dynamics of a limited liquid volume. *Kiev: Institute of Mathematics.* (in Russian).

[26] MIKISHEV, G.I.: 1978 Experimental methods in the dynamics of spacecraft. Moscow:Mashinostroenie (in Russian).

[27] MIKISHEV, G.I. & CHURILOV, G.A.: 1977 Some results on experimental determining the hydrodynamic coefficients for cylinder with ribs. *In Book: "Dynamics of elastic and rigid bodies interaction with a liquid"*. Tomsk: Tomsk University, 31-37.

[28] MILES, J.W. 1984 Internally resonant surface waves in circular cylinder. *J. Fluid Mech.* **149**, 1-14.

[29] MILES, J.W. 1984 Resonantly forces surface waves in circular cylinder. *J. Fluid Mech.* **149**, 15-31.

[30] MOISEYEV, N.N.: 1958. To the theory of nonlinear oscillations of a limited liquid volume. *Applied Mathematics and Mechanics (PMM)*, **22**, 612-621 (in Russian).

[31] NARIMANOV, G.S.: 1957 Movement of a tank partly filled by a fluid: the taking into account of non-smallness of amplitude. *Journal of Applied Mathematics and Mechanics (PMM)*, **21**, 513-524 (in Russian).

[32] NARIMANOV, G.S., DOKUCHAEV, L.V.& LUKOVSKY, I.A.: 1977 Nonlinear dynamics of flying apparatus with liquid. Moscow: Mashinostroenie, 1977, 203pp. (in Russian).

[33] OCKENDON, H., OCKENDON, J.R.& WATERHOUSE, D.D. 1996 Multi-mode resonance in fluids. *J. Fluid Mech.* **315**, 317–344.

[34] MOISEYEV, N.N.& RUMYANTSEV, V.V.: 1968 Dynamic stability of bodies containing fluid. Springer, New York.